

Undercoordination-driven real-bond Goldschmidt-Pauling contraction and the inter-electron-pair Coulomb repulsion stiffening molecular clusters, surface skins, and ultrathin films of water

Chang Q Sun,^{1,3,4} Xi Zhang,¹ Ji Zhou,² Yongli Huang,³ Yichun Zhou,³ and Weitao Zheng⁴

¹ School of Electrical and Electronic Engineering, Nanyang Technological University, Singapore 639798

² Key Laboratory of Low-Dimensional Materials and Application Technologies, and Faculty of Materials and Optoelectronics and Physics, Xiangtan University, Hunan 411105, China

³ State Key Laboratory of New Ceramics and Fine Processing, Department of Materials Science and Engineering, Tsinghua University, Beijing 100084, China

⁴ School of Materials Science, Jilin University, Changchun 130012, China

A slight, molecular-undercoordination-induced, Goldschmidt-Pauling contraction of the stiffer “ $\text{O}^{2-}\text{-H}^{+/p}$ ” real-bond and a significant, inter-electron-pair Coulomb-repulsion-driven, elongation of the softer “ $\text{H}^{+/p}\text{:O}^{2-}$ ” non-bond, and the associated stiffness relaxation, of the segmented “ $\text{O}^{2-}\text{:H}^{+/p}\text{-O}^{2-}$ ” bond, are recognized as the key to stiffening $(\text{H}_2\text{O})_N$ molecular clusters, surface skins, and ultrathin films of water. Agreement between calculations and measurements verified our expectations that the shortened-and-stiffened real-bond stiffens the stiffer phonons ($>3000\text{ cm}^{-1}$), densifies bonding electrons, entraps binding energy, and elevates the melting point and hence the viscosity, surface tension, and elasticity, and that the lengthened-and-softened non-bond softens the softer phonons ($<300\text{ cm}^{-1}$), expands the volume, and polarizes the electron pairs of the undercoordinated molecules in freestanding and encapsuled clusters, water surfaces, and ultrathin films that exhibit ice- or glue-like and hydrophobic nature at the ambient. This effect becomes more significant as N is reduced.

PACS numbers: 61.20.Ja, 61.30.Hn, 68.08.Bc

Size (N) reduction of $(\text{H}_2\text{O})_N$ clusters makes the anomalous H_2O even more fascinating [1-12]. When water turns to be monomers, the O 1s binding energy shifts from 538.1 to 539.8 eV (see Fig S1) [13, 14] and the stiffer O-H stretching phonons ω_{H} shifts from 3200 to 3650 cm^{-1} (Fig S2) with the surface component at 3400 cm^{-1} [15, 16]. The undercoordination-induced stiffer phonon stiffening and O 1s binding energy entrapping are associated with O---O expansion, by up to 5.9% [1, 17-20], charge entrapment [7, 21-23], charge densification [6, 8, 9, 22, 24, 25], and charge polarization [10], etc., for water clusters. Size-reduction also enhances the thermal-stiffening of the stiffer ω_{H} (Fig S3) [26] and compensates for the pressure-softening of the ω_{H} (Fig S4) [27]. Water encapsulated in nanopores [28, 29] or a mono- or bi-layer of water films on graphite, silica, and metals [4, 5, 30-34] perform more ice- or glue-like (as indication of melting point elevation) under the ambient conditions, except for hydrophilic contact inside nanopores [35] or wetting with hydrophilic topologic configurations [36]. The rate of the pressure-driven water flow through carbon nanotubes is orders high in magnitude, faster than would be predicted from conventional fluid-flow theory. The thinner of the channel diameter is, the faster the flow rate of the fluid will be [37, 38]. A monolayer film of water at room temperature manifests “quasi-solid” and hydrophobic nature that prevents the monolayer water from being wetted by a water droplet [34].

With respect to the advancement in the study of $(\text{H}_2\text{O})_N$ clusters [11, 39-43], as mentioned above, clarification of the physical origin and correlation between the molecular undercoordination, hydrogen bond relaxation, and importantly, the forces driving the excessive anomalies of $(\text{H}_2\text{O})_N$ clusters remain great challenge. Incorporating the density functional theory (DFT) calculations into vibration and electron emission spectroscopic measurements, we show that the molecular-undercoordination-induced shortening-and-stiffening of the “ $\text{O}^{2-}\text{-H}^{+/p}$ ” real-bond and the inter-electron-pair Coulomb-repulsion-driven lengthening-and-softening of the “ $\text{H}^{+/p}\text{:O}^{2-}$ ” non-bond in the master-slave-segmented “ $\text{O}^{2-}\text{:H}^{+/p}\text{-O}^{2-}$ ” bond [44] triggers these anomalies.

Figure 1 shows the “ $\text{O}^{2-}\text{:H}^{+/p}\text{-O}^{2-}$ ” (H) bond [44], with indication of forces acting on the electron pairs, as the basic structural unit for O---O interaction in solid and liquid H_2O of various topologies. As the coordination origin, $\text{H}^{+/p}$ donates its electron to the right O^{2-} to form the real-bond and meanwhile it is polarized by the nonbonding electron lone pair of O^{2-} . This H-bond can

be segmented into a shorter, stronger, and stiffer (~ 0.10 nm, ~ 4.0 eV/bond, > 3000 cm^{-1}) intramolecular $\text{H}^{+/p}\text{-O}^{2-}$ real-bond with exchange interaction and a longer, weaker, and softer (~ 0.20 nm, ~ 0.05 eV/bond, < 300 cm^{-1}) intermolecular $\text{O}^{2-}:\text{H}^{+/p}$ non-bond with van der Waals interaction. The often overlooked Coulomb repulsion between the unevenly bound electron pairs and the segmental disparity dictate the dynamics of corporative relaxation of the segments in length and stiffness. The response of the segmental length and the stiffness to the applied stimuli forms the key to the anomalies of water ice.

According to the bond order-length-strength (BOLS) correlation premise [45-48], bond order loss shortens and strengthens the remnant bonds of undercoordinated atoms with an association of local densification and quantum entrapment of the binding energy and the bonding and core electrons, irrespective of the nature of the bond or the structure phase of the specimen:

$$\begin{cases} C_z = 2\{1 + \exp[(12 - z)/(8z)]\}^{-1} & (\text{bond} - \text{contraction} - \text{coefficient}) \\ C_z^{-m} = E_z / E_b & (\text{bond} - \text{strengthening} - \text{coefficient}) \end{cases} \quad (1)$$

where z is the effective coordination number (CN) and m the bond nature indicator. The locally and densely entrapped bonding charge in turn polarizes the nonbonding electrons [47], which are responsible for the creation of Dirac-Fermi polarons at graphene zigzag edges [49] and the emerging catalytic enhancement and dilute magnetism of noble metals [50] and ZnO [51] at the nanoscale.

The monolayer and the surface skin of water, the encapsuled and the free-standing $(\text{H}_2\text{O})_N$ clusters should share the same entity of bond order deficiency to follow the BOLS premise. However, the isolation of each molecule by the weakly bound electron lone pairs differentiates water from other materials in implementing the BOLS correlation. The segmental disparity in binding energy and the presence of the inter-electron-pair Coulomb repulsion break the generality of the BOLS for water. However, they make the real-bond as the ‘master’ to contract lesser than eq(1) expected and force the other ‘slave’ non-bond into the Coulomb-repulsion-driven lengthening and weakening.

If we average the surrounding interactions by other H₂O molecules or protons as the background and ignore the nucleus quantum effect on fluctuations [52], there are three forces acting on each of the electron pairs, see Figure 1 :

- (i) Coulomb repulsion between the unevenly-bound electron pairs, $f_q \propto (d_{O\cdots O})^{-2}$, points away from the H^{+/p}.
- (ii) The force of recovery of segment relaxation, $f_{rx} = -k_x \Delta d_x$. The force constant k_x approximates the second differentiation of the respective interatomic potential at equilibrium.
- (iii) The force driving undercoordination-induced length contraction, f_{dx} ($x = L$ and H for the low- and the high-frequency of vibration), points towards the H^{+/p}. The magnitude of the f_{dx} varies with coordination conditions and the strength of the specific segment.

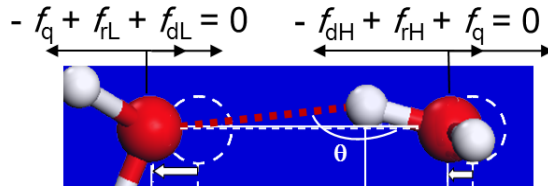


Figure 1 Interactions, forces, and relaxation dynamics of the master-slave-segmented “O²⁻:H^{+/p}-O²⁻” bond. H^{+/p} is the coordination origin. f_q is the inter-electron-pair Coulomb repulsion, f_{dx} is driving force for the molecular-undercoordination-induced contraction ($x = H, L$ for the segment of high- and low-frequency vibration), and f_{rx} the dislocation recovery force. The resultant of these force determines the relaxation dynamics of the segmented H bond in length d_L and d_H and the angle θ .

Because of its rather weak interaction, the O²⁻:H^{+/p} binding energy contributes insignificantly to the Hamiltonian or the atomic cohesive energy and hence the associated quantities. Thus, any detectable quantity (q) of a specimen depends functionally on the order, length, and energy of the representative real-bond of the specimen, and the associated electron entrapment and polarization. For (H₂O)_N clusters, the volume, the binding energy in x-ray photoelectron spectrum, the critical temperature of phase transition, the charge entrapment, densification and

polarization, and the stiffness of the corresponding Raman phonons of a $(\text{H}_2\text{O})_N$ specimen follow the given relations [48]:

$$\left. \begin{array}{l} V_{\text{H}_2\text{O}} \\ \rho_q \\ \Delta E_c \\ T_C \\ \Delta \omega_x \end{array} \right\} \propto \left\{ \begin{array}{ll} d_{O-O}^3 & (\text{molecular – volume}) \\ d_H^{-1} & (\text{bonding-charge-densification}) \\ E_H & (\text{core – level – shift; potential – trap – depth}) \\ E_H & (\text{critical – temperature for phase transition}) \\ \sqrt{E_x} d_x^{-1} \cong \sqrt{Y_x d_x} & (\text{phonon – frequency – shift} = \sqrt{\text{bond stiffness}}) \end{array} \right. \quad (2)$$

E_x ($x = L, H$) is the respective cohesive energy. It can be derived that the phonon frequency shift is proportional to the square root of the bond stiffness being the product of the Young's modulus ($Y_x \propto E_x d_x^{-3}$) and the bond length. Theoretical reproduction of the pressure-depressed T_C for ice VII-VIII phase transition has confirmed that the real-bond energy dictates the T_C with derivative of the H-O bond energy of 3.97 eV, being twice that of the C-C bond in diamond (1.84 eV) [44].

Figure 1 also illustrates our expectations on the segmental cooperative relaxation dynamics of the H-bond. Water-cluster size reduction will shorten and stiffen the real-bond, of which the bonding electron pair pushes the lone electron pair of the non-bond away from the $\text{H}^{+/P}$ origin through Coulomb repulsion, and hence the non-bond expands and softens. This process is opposite to that happened to the H-bond of ice under compression [44]. The weaker non-bond always relaxes more in length than the stronger real-bond. The extent of relaxation will increase as the N is reduced, according to BOLS premise.

In order to verify the hypotheses and expectations on the relaxation dynamics of the angle, length, and stiffness of the segmented H-bond of water clusters under the atmospheric pressure, we calculated the optimal cluster structures and the respective vibration spectra as a function of cluster size (see Fig. S5[16]). Geometry optimizations of $(\text{H}_2\text{O})_N$ clusters were performed in Dmol³ code using Perdew-Wang (PW91) form [53] of functional in general gradient approximation (GGA). All-electron method was adopted including core electrons in calculation with a double numeric plus polarization basis set to approximate the wave functions. During calculations, the self-consistency threshold of total energy is set at 10^{-6} Hartree. In the geometry

optimization, the tolerance limits for the energy, force and displacement are set at 10^{-5} Hartree, 0.002 Hartree/Å and 0.005 Å, respectively. Harmonic vibrational frequencies are computed by diagonalizing the mass-weighted Hessian matrix [54].

Figure 2 (see Table S1[16]) shows indeed that the $(\text{H}_2\text{O})_N$ size reduction from $N = 20$ to 2 shortens the $\text{O}^{2-}\text{-H}^{+/p}$ and lengthens the $\text{H}^{+/p}\text{:O}^{2-}$ (Fig. 2a), and relaxes the bond angle (Fig. 2b) as well, non-monotonously because of the change of the effective CNs in the configurations [16]. DFT calculations confirmed three optimal structures, as detected recently [12], for $N = 6$ (Fig S5 [16]) configurations. The 6-cage structure possesses the lowest cohesive energy of -458.7191 eV, being 0.0003 eV lower than that of the 6-book and 0.0009 eV lower than that of the 6-prism.

Calculations turns out that the $\text{H}^{+/p}\text{-O}^{2-}$ contracts by 4.0% from 0.101 nm for the bulk water to 0.097 nm for a monomer and $\text{O}^{2-}\text{:H}^{+/p}$ expands by 8.6% from 0.175 for bulk to 0.190 nm for a dimer. The N-reduction induced asymmetric relaxation allows us to focus on the lower end of cluster size ($N \leq 6$, monotonous trend) with monotonous changing trend, subsequently, without influencing the generality of conclusions.

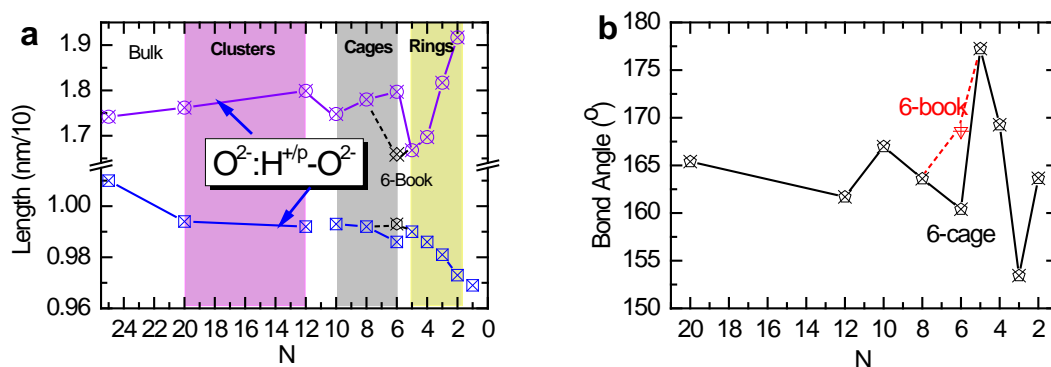


Figure 2 DFT-derived (a) d_L and d_H asymmetric relaxation and (b) bond angle θ variation as a function of $(\text{H}_2\text{O})_N$ cluster size. As N decreases, the $\text{H}^{+/p}\text{-O}^{2-}$ real-bond contracts associated with the $\text{O}^{2-}\text{:H}^{+/p}$ non-bond elongation, resulting in the $\text{O} \cdots \text{O}$ distance and molecular volume expansion. The length and angle relaxation of the 6-cage and the 6-book structures are indicated. The non-monotonous profiles result from the effective CNs of the optimal structural configurations (Fig. S5[16]).

Figure 3a shows the cluster size dependence of the vibration spectra of $(\text{H}_2\text{O})_N$ with respect to that of ice Ih phase. As expected, N reduction stiffens the stiffer $\text{H}^{+/p}\text{-O}^{2-}$ stretching phonons ω_H and meanwhile softens the softer $\text{O}^{2-}\text{:H}^{+/p}$ stretching mode ω_L from 250 to 170 as the water turns to be dimers. The $\text{O}^{2-}\text{:H}^{+/p}\text{-O}^{2-}$ bending mode ω_{B1} (400-1000 cm^{-1}) shifts slightly but the $\text{H}^+\text{-O}^{2-}\text{-H}^+$ bending mode ω_{B2} ($\sim 1600 \text{ cm}^{-1}$) remains silent, as experimentally confirmed [26]. The trend of stiffer ω_H stiffening in Figure 3b is consistent with experimental measurements (Fig S3) [16]. For instances, the ω_H is stiffened from 3200 to 3650 cm^{-1} when water cluster $(\text{H}_2\text{O})_N$ drops from $N = 6$ to 1 [16, 55] and from 3420 to 3650 cm^{-1} when the water (surface) becomes gaseous molecules [56]. Recent infra-red spectroscopy measurements [15, 16, 57] revealed that the ω_H shifts from 3225, 3350, 3380 to 3525 cm^{-1} when N drops from 6, 5, 4 to 3 of $(\text{H}_2\text{O})_N$ encapsuled in inert matrices. The frequency changes slightly by 5-10 cm^{-1} when the clusters are in Ke and Ar matrices.

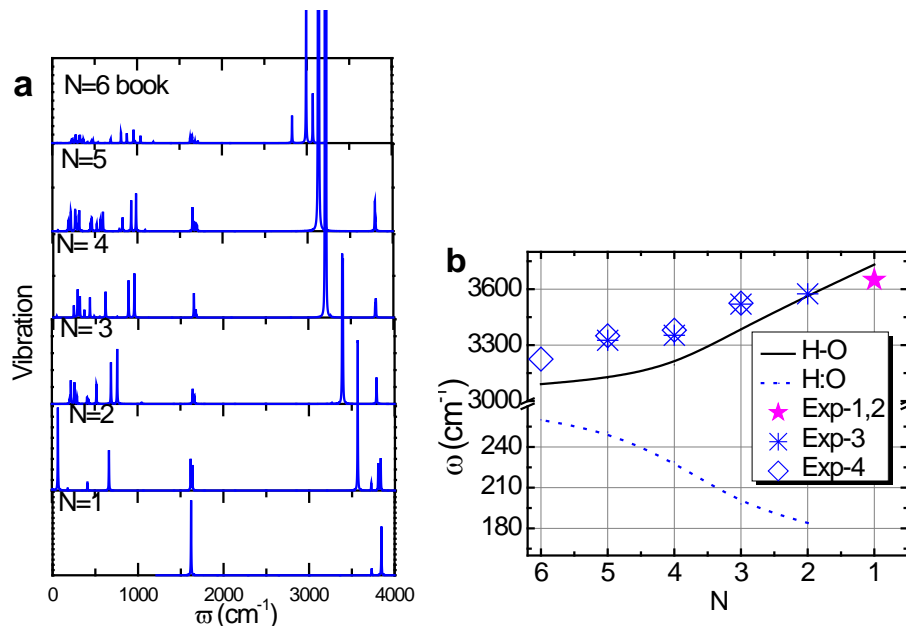


Figure 3 Size-induced asymmetric phonon relaxation of $(\text{H}_2\text{O})_N$ clusters ($N \leq 6$). N reduction stiffens the $\text{H}^{+/p}\text{-O}^{2-}$ stretching phonons at ω_H ($>3000 \text{ cm}^{-1}$) and softens the $\text{O}^{2-}\text{:H}^{+/p}$ stretching mode ω_L ($<300 \text{ cm}^{-1}$). Scattered datum are measurements of Exp-1 [56], Exp-2 [55], Exp-3 [15] and Exp-4 [57].

Figure 4a plots the calculated O---O distance (from Fig. 2) as a function of cluster size. Reducing N from 20 to 5 and 3, the O---O distance expands by 1.3%, and 1.8%, with a volume expansion of 4.1 and 5.6%, respectively. The latter is exactly the case (5.9%) measured at 25°C from water surface [19]. Figure 4 b shows the anticipated T_{mN} elevation and ΔE_{1sN} entrapment. According to Eq (1), the T_{mN} and the O 1s energy shift are both proportional to the real-bond energy,

$T_{mN}/T_{mBulk} = \Delta E_{1sN}/\Delta E_{1sBulk} = (d_{HN}/d_{HBulk})^{-m} = C_H^{-4}$, ($m = 4$ for the real-bond in H_2O [48]). Based on the derived $H^{+/p}-O^{2-}$ length (see Table S1[16]), we found that when the N is reduced from infinitely large to 5 and 2, the T_m will increase by 4.4% and 12% to 285 (N = 5) and 305 K (N = 2), which explains why the monolayer water is glue- or ice- like at the ambient. Water manifests high viscosity or “quasi-solid” nature when it is cooled approaching T_m .

The strengthening of the $H^{+/p}-O^{2-}$ real-bond is associated with the interatomic potential-well depression, which shifts the E_{1sN} from that of an isolated O atom $E_{1s(0)}$ in the form of [48]:

$$\frac{E_{1sN} - E_{1s(0)}}{E_{1sBulk} - E_{1s(0)}} = C_{HN}^{-4} \quad (3)$$

The bind energy is expected to be entrapped further by 20% if the bulk water turns to be monomers. It has been measured that the O E_{1s} shifts from 538.2 to 538.6 eV when the water cluster size is reduced from N = 200 to 40 and up to 539.8 eV for the free water molecules [13, 27]. The O E_{1s} of water surface was found dominated by a main peak centered at 538.1 eV with an ice bulk satellite at 536.6 eV with respect to the peak at 539.9 eV for gaseous phase [16, 58].

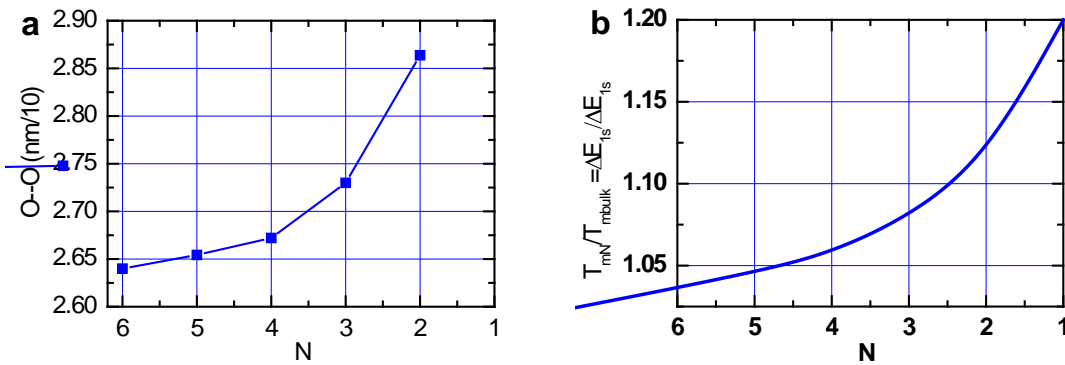


Figure 4 DFT-derived (solid lines) size dependence of (a) O---O distance and (b) melting point, T_m , elevation and O 1s binding energy entrapment.

The polarization of water molecules at the surface or in the clusters [10, 59] is related to the molecule volume expansion because of the conservation of molecular charge. An ultrafast liquid-jet vacuum ultra-violet photoelectron spectroscopy [6] revealed that the bound (vertical binding) energies for the solvated electrons at the water surface are 1.6 eV and in the bulk solution they are 3.3 eV and that the bound energy decreases with water cluster size. These findings evidence the undercoordination-induced polarization that lowers the work function of the bound electrons.

The enhanced surface polarization also contribute to the viscosity and elasticity (both surface tension and elastic modulus are proportional to the binding energy density in addition to the contribution of polarization [60]). Surface polarization and the enhanced elasticity of the surface covering sheet has been identified as the essential conditions for the hydrophobicity and lubricity of the surface, and therefore, it is not surprising that the ultrathin water films are hardly wetted by a water droplet [34].

Trend consistency between DFT calculations and the XPS and Raman measurements has thus verified our hypothesis and expectations, and the validity of the DFT that may be subject to further improvement in accuracy, on the excessive anomalies of water clusters that have been clarified as follows:

- (i) The often overlooked molecular-undercoordination-induced Goldschmidt-Pauling real-bond contraction and the inter-electron-pair Coulomb repulsion driven non-bond elongation and polarization are recognised as the key to the excessive anomalies of water molecular clusters.
- (ii) The shortened-and-stiffened real-bond stiffens the stiffer phonons, densifies and entraps bonding electrons and binding energy, and elevates the melting point and viscosity.
- (iii) The lengthened-and-softened non-bond softens the softer phonons, expands the volume, and polarizes the electron pairs of the undercoordinated molecules in freestanding and encapsuled clusters, water surface, and ultrathin films that exhibit ice-or glue-like and hydrophobic nature at room temperature.

Financial support from NSF (Nos.: 21273191, 1033003, 90922025) China is acknowledged.

References

Contacting authors: zhouji@tsinghua.edu.cn; [wtzheng@jlu.edu.cn](mailto:wz Zheng@jlu.edu.cn); ecqsun@ntu.edu.sg; CQ is affiliated with honorary appointments at 3 and 4

- [1] K. Liu, J. D. Cruzan, and R. J. Saykally, *Science* **271**, 929 (1996).
- [2] G. N. I. Clark, C. D. Cappa, J. D. Smith, R. J. Saykally, and T. Head-Gordon, *Mol. Phys.* **108**, 1415 (2010).
- [3] R. Ludwig, *Angew. Chem. Int. Ed.* **40**, 1808 (2001).
- [4] A. Michaelides, and K. Morgenstern, *Nat. Mater.* **6**, 597 (2007).
- [5] K. Xu, P. G. Cao, and J. R. Heath, *Science* **329**, 1188 (2010).
- [6] K. R. Sieferrmann, Y. Liu, E. Lugovoy, O. Link, M. Faubel, U. Buck, B. Winter, and B. Abel, *Nat Chem* **2**, 274 (2010).
- [7] L. Turi, W. S. Sheu, and P. J. Rossky, *Science* **309**, 914 (2005).
- [8] J. R. R. Verlet, A. E. Bragg, A. Kammrath, O. Cheshnovsky, and D. M. Neumark, *Science* **307**, 93 (2005).
- [9] N. I. Hammer, J. W. Shin, J. M. Headrick, E. G. Diken, J. R. Roscioli, G. H. Weddle, and M. A. Johnson, *Science* **306**, 675 (2004).
- [10] J. K. Gregory, D. C. Clary, K. Liu, M. G. Brown, and R. J. Saykally, *Science* **275**, 814 (1997).
- [11] F. N. Keutsch, and R. J. Saykally, *PNAS* **98**, 10533 (2001).
- [12] C. Perez, M. T. Muckle, D. P. Zaleski, N. A. Seifert, B. Temelso, G. C. Shields, Z. Kisiel, and B. H. Pate, *Science* **336**, 897 (2012).
- [13] M. Abu-Samha, K. J. Borge, M. Winkler, J. Harnes, L. J. Saethre, A. Lindblad, H. Bergersen, G. Ohrwall, O. Bjorneholm, and S. Svensson, *J. Phys. B* **42**, 055201 (2009).
- [14] K. Nishizawa, N. Kurahashi, K. Sekiguchi, T. Mizuno, Y. Ogi, T. Horio, M. Oura, N. Kosugi, and T. Suzuki, *PCCP* **13**, 413 (2011).
- [15] J. Ceponkus, P. Uvdal, and B. Nelander, *J Phys Chem A* **116**, 4842 (2012).
- [16] (Supplementary Information).
- [17] M. Abu-Samha, and K. J. Borge, *J. Chem. Phys.* **128**, 154710 (2008).
- [18] K. R. Wilson, B. S. Rude, T. Catalano, R. D. Schaller, J. G. Tobin, D. T. Co, and R. J. Saykally, *J. Phys. Chem. B* **105**, 3346 (2001).
- [19] K. R. Wilson, R. D. Schaller, D. T. Co, R. J. Saykally, B. S. Rude, T. Catalano, and J. D. Bozek, *J. Chem. Phys.* **117**, 7738 (2002).
- [20] A. Lenz, and L. Ojamae, *J. Chem. Phys.* **131**, 134302 (2009).
- [21] R. Vacha, O. Marsalek, A. P. Willard, D. J. Bonthuis, R. R. Netz, and P. Jungwirth, *J Phys Chem Lett* **3**, 107 (2012).
- [22] O. Marsalek, F. Uhlig, T. Frigato, B. Schmidt, and P. Jungwirth, *Phys. Rev. Lett.* **105**, 043002 (2010).
- [23] F. Baletto, C. Cavazzoni, and S. Scandolo, *Phys. Rev. Lett.* **95**, 176801 (2005).
- [24] S. Liu, J. Luo, G. Xie, and D. Guo, *J. Appl. Phys.* **105**, 124301 (2009).
- [25] D. H. Paik, I. R. Lee, D. S. Yang, J. S. Baskin, and A. H. Zewail, *Science* **306**, 672 (2004).

- [26] S. A. Deshmukh, S. K. Sankaranarayanan, and D. C. Mancini, *J Phys Chem B* **116**, 5501 (2012).
- [27] O. Bjorneholm, F. Federmann, S. Kakar, and T. Moller, *J. Chem. Phys.* **111**, 546 (1999).
- [28] M. L. Lakhanpal, and B. R. Puri, *Nature* **172**, 917 (1953).
- [29] L. Li, Y. Kazoe, K. Mawatari, Y. Sugii, and T. Kitamori, *J Phys Chem Lett*, 2447 (2012).
- [30] P. B. Miranda, L. Xu, Y. R. Shen, and M. Salmeron, *Phys. Rev. Lett.* **81**, 5876 (1998).
- [31] F. McBride, G. R. Darling, K. Pussi, and A. Hodgson, *Phys. Rev. Lett.* **106**, 226101 (2011).
- [32] A. Hodgson, and S. Haq, *Surf. Sci. Rep.* **64**, 381 (2009).
- [33] S. Meng, E. G. Wang, and S. W. Gao, *Phys Rev B* **69**, 195404 (2004).
- [34] C. Wang, H. Lu, Z. Wang, P. Xiu, B. Zhou, G. Zuo, R. Wan, J. Hu, and H. Fang, *Phys. Rev. Lett.* **103**, 137801 (2009).
- [35] F. G. Alabarse, J. Haines, O. Cambon, C. Levelut, D. Bourgogne, A. Haidoux, D. Granier, and B. Coasne, *Phys. Rev. Lett.* **109**, 035701 (2012).
- [36] Q. Z. Yuan, and Y. P. Zhao, *Proc. R. Soc. A-Math. Phys. Eng. Sci.* **468**, 310 (2012).
- [37] M. Whitby, L. Cagnon, M. Thanou, and N. Quirke, *Nano Lett.* **8**, 2632 (2008).
- [38] X. C. Qin, Q. Z. Yuan, Y. P. Zhao, S. B. Xie, and Z. F. Liu, *Nano Lett.* **11**, 2173 (2011).
- [39] F. Y. Li, L. Wang, J. J. Zhao, J. R. H. Xie, K. E. Riley, and Z. F. Chen, *Theor. Chem. Acc.* **130**, 341 (2011).
- [40] C. Vega, J. L. F. Abascal, M. M. Conde, and J. L. Aragoes, *Faraday Discuss.* **141**, 251 (2009).
- [41] D. Kang, J. Dai, Y. Hou, and J. Yuan, *J. Chem. Phys.* **133**, 014302 (2010).
- [42] R. Shishido, J. L. Kuo, and A. Fujii, *J. Phys. Chem. A* **116**, 6740 (2012).
- [43] K. Mizuse, J. L. Kuo, and A. Fujii, *Chemical Science* **2**, 868 (2011).
- [44] C. Q. Sun, X. Zhang, and W. T. Zheng, *Chem Sci* **3**, 1455 (2012).
- [45] L. Pauling, *J. Am. Chem. Soc.* **69**, 542 (1947).
- [46] V. M. Goldschmidt, *Ber Deut Chem Ges* **60**, 1263 (1927).
- [47] C. Q. Sun, *Nanoscale* **2**, 1930 (2010).
- [48] C. Q. Sun, *Prog. Solid State Chem.* **35**, 1 (2007).
- [49] W. T. Zheng, and C. Q. Sun, *Energy & Environ Sci* **4**, 627 (2011).
- [50] E. Roduner, *Chem. Soc. Rev.* **35**, 583 (2006).
- [51] J. W. Li, S. Z. Ma, X. J. Liu, Z. F. Zhou, and C. Q. Sun, *Chem. Rev.* **112**, 2833 (2012).
- [52] X. Z. Li, B. Walker, and A. Michaelides, *PNAS* **108**, 6369 (2011).
- [53] J. P. Perdew, and Y. Wang, **45**, 13244 (1992).
- [54] E. B. Wilson, J. C. Decius, and P. C. Cross, *Molecular Vibrations* (Dover, New York, 1980).
- [55] Q. Sun, *Vib. Spectrosc* **51**, 213 (2009).
- [56] P. C. Cross, J. Burnham, and P. A. Leighton, *J. Am. Chem. Soc.* **59**, 1134 (1937).
- [57] S. Hirabayashi, and K. M. T. Yamada, *J. Mol. Struct.* **795**, 78 (2006).
- [58] B. Winter, E. F. Aziz, U. Hergenhausen, M. Faubel, and I. V. Hertel, *J. Chem. Phys.* **126**, 124504 (2007).
- [59] F. Yang, X. Wang, M. Yang, A. Krishtal, C. van Alsenoy, P. Delarue, and P. Senet, *Physical chemistry chemical physics : PCCP* **12**, 9239 (2010).
- [60] M. Zhao, W. T. Zheng, J. C. Li, Z. Wen, M. X. Gu, and C. Q. Sun, *Phys Rev B* **75**, 085427 (2007).

